Silicon Nitride Capacitive Chemical Sensor for Phosphate Ion Detection Based on Copper Phthalocyanine – Acrylate-polymer

Lassaad Barhoumi,[a, b] Abdoullatif Baraket,*[d] Naglaa Mohammed Nooredeen,[c] Mounir Ben Ali,[a, b], Mohammed Nooredeen Abbas,[e] Joan Bausells,[f] and Abdelhamid Errachid[d]

[a] L. Barhoumi, M. B. Ali, University of Sousse, Higher Institute of Applied Sciences and Technology of Sousse, GREENS-ISSAT, Cit Ettafala, 4003 Ibn Khaldoun Sousse, Tunisia.
[b] L. Barhoumi, M. B. Ali, NANOMESENE Lab, LR16CRMN01, Centre for Research on Microelectronics and Nanotechnology of Sousse, Technopole of Sousse B. P. 334, Sahloul, 4034, Sousse, Tunisia.
[c] N. M. Nooredeen, Polymer and Pigments Department, National Research Centre, Cairo, Egypt.
[d] A. Baraket, A. Errachid, Université de Lyon, Institut des Sciences Analytiques, UMR 5280, CNRS, Université Lyon 1, ENS Lyon - 5, rue de la Doua, F-69100 Villeurbanne, France. E-mail: abdoullatif.baraket@isa-lyon.fr.
[e] M. N. Abbas, Analytical Laboratory, National Research Centre, Cairo, Egypt.
[f] J. Bausells, Centro Nacional de Microelectrnica (CSIC), Campus UAB, 08193 Bellaterra, Spain.

Abstract

In this work, we report the development of a highly sensitive capacitance chemical sensor based on a copper C,C,C,C-tetra-carboxylic phthalocyanine-acrylate polymer adduct (Cu(II)TCPc-PAA) for phosphate ions detection. A capacitance silicon nitride substrate based AlCu/Si-p/SiO_2/Si_3N_4 structure was used as transducer. These materials have provided good stability of electro- chemical measurements. The functionalized silicon-based transducers with a Cu(II)Pc-PAA membrane were characterized by using Mott-Schottky technique measurements at different frequency ranges and for different phosphate concentrations. The morphological surface of the Cu(II) Pc-PAA modified silicon-nitride based transducer was characterized by contact angle measurements and atomic force microscopy. The pH effect was also investigated by the Mott-Schottky technique for different Tris-HCl buffer solutions. The sensitivity of silicon nitride was e studied at different pH of Tris-HCl buffer solutions. This pH test has provided a sensitivity value of 51 mV/decade. The developed chemical sensor showed a good performance for phosphate ions detection within the range of 10^{-10} to 10^{-5} M with a Nernstian sensitivity of 27.7 mV/decade. The limit of detection of phosphate ions was determined at 1 nM. This chemical sensor was highly specific for phosphate ions when compared to other interfering ions as chloride, sulfate, carbonate and perchlorate. The present capacitive chemical sensor is thus very promising for sensitive and rapid detection of phosphate in environmental applications.

Keywords: Capacitive chemical sensor · phthalocyanine-acrylate · phosphate ions · Mott-Schottky

1. Introduction

The global demand for minerals and metals is always permanent, and this in turn is causing growing concerns about long-term environmental security. Phosphate is widely used for agriculture in the world because it is an essential nutrient. This is what makes the global consumption of phosphate raise from 43.7 million tons in 2015 to 48.2 million tons expected to be consumed in 2019 [1]. The economic geography of the world phosphate industry has been changed over the past two decades regarding the phosphate consumption. The USA was the leading producer of phosphate in 1989 (50 million tonnes), covering the 30.2% of world production. The Soviet Union was next with 37.5 million tonnes (22.8%), followed by China (12.1%) and Morocco (11%). About 35 other countries shared the remaining production, and Kazakhstan, Egypt, Jordan, Togo, Tunisia, Peru, Russia and Brazil resulted the most prominent [2]. Phosphate mining is considered the main cause of many diseases, such as allergies, respiration, dental fluorosis, stress, cardiovascular and cancer. The latter represent the primary environmental cause of mortality, especially as regards children and phosphate miners [3]. These diseases are directly related to the installation of the industrial sector of phosphate mines in addition to deforestation and the ecosystem degradation.

Therefore, chemical sensors are of growing importance in environmental analysis, especially in monitoring liquid quality. These sensors are common for the selective detection of ions, especially for applications of monitoring small organic pollutants in water. These devices can continuously and selectively detect the levels of phosphate in aqueous solution [4], in order to monitor the levels of toxic substances, such as phosphate. These chemical sensors have found numerous applications in different fields like environmental monitoring, where eutrophication is a problem caused in part by leaching inorganic phosphate into farmland an streams [5]. Phosphate is also used in biomedical research, clinical chemistry and pharmacology [6, 7].

Recently, the class of metallo-phthalocyanine (MPc) materials, which have a metal atom located in the central cavity [8], have been of great interest due to their excellent electronic properties and potential applications for the detecting targeted ions [9]. The response of sensors based on MPcs doping as sensitive membrane electrodes is believed to be based on the coordination of the analyte ion as an axial ligand with the metal center of the carrier molecule. Changing the central metal of these complexes strongly influences their selectivity [8, 10]. The MPcs were widely used in a lot of fields, such as gas sensors [11] and biosensors [12, 13], and receive a considerable attention because of the increasing importance as chemical sensors [14, 15] especially for the detection of toxic anions. Moreover, the MPcs provide high chemical and thermal stability as well as a tendency to form highly ordered layers that positively influence the device efficiency [16]. This new nanomaterial was used to develop the present chemical sensor for phosphate detection. This material is compatible with integrated circuit technology (IC) and has been used in chemical sensors [17, 18].

Moreover, the covalent binding of the ionophore C,C,C,C-tetra-carboxylic phthalocyanine-acrylate polymer adduct (Cu(II)TCPc-PAA) gives long-term stability by preventing the ionophore from leaching into the sample solution, crystallizing or evaporating. Furthermore, this ionophore improves the sensor selectivity and detection limit [19].

In this work, we study a new synthesized copper, C,C,C,C-tetra-carboxylic acid- polyacrylamide (Cu(II)Pc-PAA) as a selective ionophore for phosphate [20]. In this context, a novel electrochemical capacitive sensors based on AlCu/Si-p/SiO$_2$/Si$_3$N$_4$ substrates and functionalized with copper phthalocyanine derivative have been developed. The modified transducer surfaces have been characterized using contact angle measurements and Atomic Force Microscopy (AFM). The capacitive sensor response towards phosphate ions has been tested in high (10 kHz) and low (100 Hz) frequencies using Mott-Schottky electrochemical technique.

2. Experimental Details

2.1. Material

Tetrahydrofuran (THF) was obtained from Fluka Analytical, France. Dimethyl sulfoxide (DMSO), Tris(hydroxymethyl) aminomethane, Hydrogen peroxide H$_2$O$_2$ (35%), sulfuric acid (H$_2$SO$_4$) and phosphate K$_2$HPO$_4$ were purchased from Sigma Aldrich France. Phosphate ions were obtained from dibasic potassium phosphate K$_2$HPO$_4$. Different solutions of the ions were prepared in aqueous medium at various concentrations. The key ionophore, which was the copper Phthalocyanine, C,C,C,C-tetra-carboxylic acid-polyacrylamide (C$_{32}$H$_{16}$N$_8$),was synthesized in the National Research Centre in Cairo(Egypt), and it was composed of four isoindoles (a benzene fused to a pyrrole ring) connected to nitrogen atoms and had a central copper atom. This new nanomaterial was used to develop the present chemical sensor for phosphate detection. All solutions were prepared in ultrapure water (Millipore 18 MW.cm) and phosphate sensors ware tested in a Tris-HCl buffer solution 0.1 M.

2.2. Instrumentation

2.2.1. Wettability

The hydrophilicity of the immobilized Cu-Pc(II)-PAA membrane was investigated by contact angle measurements using 'Digidrop' from GBX (France). 5 mL of deionized water was dropped on the sensing film surface through the application nozzle at 258C. The digital camera associated with the instrument acquired the image and analyzed the water droplet behavior. The contact angle was obtained for five different areas of a given wafer with five separated droplets and the statistical average of the five measurements was calculated. The volume and size of the drops were kept constant.

2.2.2. Atomic Force Microscopy (AFM)

The AFM characterization was performed using a Nano observer SCIEN Tec (France). The AFM Nano-Observer had a maximum scan area of 110 µm^2 and a minimum of 0.2 µm^2. The measurements were made using a silicon cantilever tip (Scien TecApp Nano). The cantilever contained a silicon tip bearing an integrated standard profile tip with a nominal spring constant at 25–75 N/m in the frequency range of 200400 KHz with a length of 125 µm, a width of 35 µm, and a thickness of 4.5 µm. The tip radius was lower than 10 nm and the tip height was 14–16 µm. The imagining was performed at 5 V of amplitude, a set point of 8 V, a tip DC at 477 nV, and a frequency of 337 kHz. These measurements were carried out in a 'tapping-mode' (TM-AFM) which was used with a speed of 0.5 line/s and a resolution of 1024 lines. Samples were analyzed in a 5µm x 5µm area.

2.2.3. Electrochemical Analysis

All electrochemical capacitance measurements were carried out at room temperature in a Faraday box, using a VMP3 potentiostat (16 channels BioLogic France) which was monitored by EC-Lab software. Mott-Schottky capacitance measurements were performed in a three-electrode electrochemical cell (Platinum counter electrode, Ag/AgCl reference electrode and a functionalized AlCu/Si-p/SiO_2/Si_3N_4 structure as a working electrode). The cell was connected to the potentiostat. The capacitance-voltage measurements were carried out within the potential range of -0.5 to 2 V at high frequency (10 kHz) and at low frequency (100 Hz) with a signal amplitude of 10 mV. All measurements were made with a 5 mL freshly prepared Tris-HCL solution (10 mM and pH=7.2).

2.3. Synthesis of Sensitive Molecule Copper Phthalocyanine

The novel phthalocyanine derivative Cu-Pc(II)-PAA (Figure 1) was synthesized in the National Research Centre of Cairo. The ionophore Copper phthalocyanine-C,C,C,C-tetra-carboxylic acid (I) and the adduct of copper phthalocyanine-C,C,C,C-tetra-carboxylic acid-PAA (II) were synthesized according to (Figure 1) and characterized by elemental analysis and UV-Vis and IR spectroscopy [21]. Briefly, the condensation of trimellitic anhydride in the presence of urea, ammonium molybdate and copper acetate was used to form the tetra-formamide phthalocyanine copper. Ionophore (I) was obtained by hydrolyzing the product in an alkaline medium. The ionophore-polymer was synthesized by condensing the carboxylic group of ionophores (I) with the NH_2 groups of PAA by refluxing it in dimethylformamide (DMF) at 150ºC in the presence of polyphosphoric acid, adopting a previously reported procedure [22].
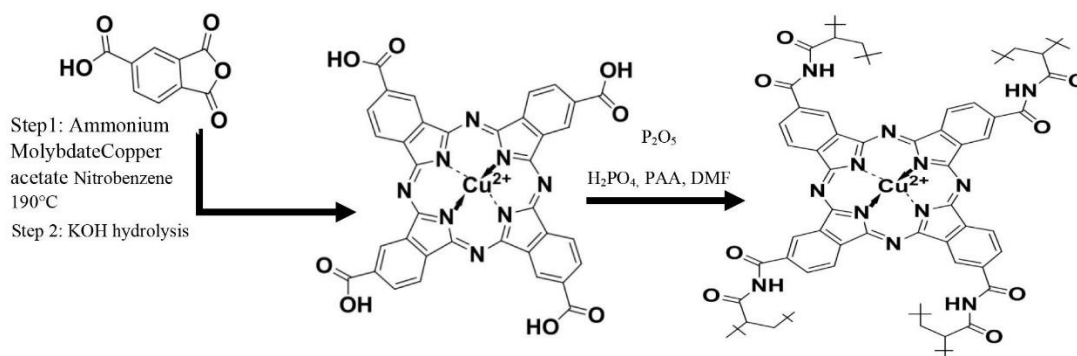

Fig. 1. Synthesis of Copper Phthalocyanine, 2,9,16,23-tetracarboxylic acid-Polyacrylamide (TCCu(II)Pc-PAA ionophore (II).

2.4 Capacitance Electrode Preparation

The planar capacitance sensor based on silicon nitride was fabricated from a p-type silicon substrate, with a <100> orientation and 4–40 $\Omega \cdot cm^1$ resistivity. A thin layer of 78 nm thickness of silicon dioxide (SiO_2) was grown thermally onto the silicon surface followed by a deposition of 100 nm of silicon nitride (Si_3N_4) prepared by Low-Pressure Chemical-Vapor Deposition (LPCVD). The electrical contact on the silicon backside was obtained by over doping it with boron ions and a deposition of 1

µm of an Al/(1%Cu) alloy. Finally, the wafers consisting of AlCu/Si-p/SiO$_2$/Si$_3$N$_4$ were diced into single chips of 1 cm^2, which presented the working electrode (Figure 2).
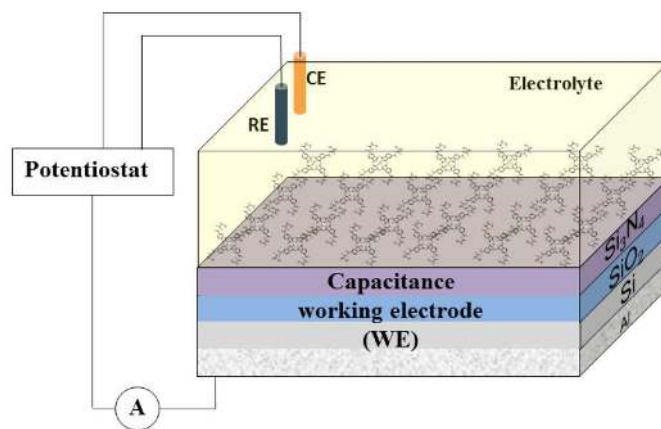

Fig. 2. Scheme of electrochemical capacitance ion sensor based on AlCu/Si-p/SiO$_2$/Si$_3$N$_4$ structure and functionalized with sensitive layer of Cu(II) Pc-PAA for phosphate ion detection.

The AlCu/Si-p/SiO$_2$/Si$_3$N$_4$ substrate was cleaned twice with acetone for 15 min by sonication, rinsed with distilled water, and finally dried under nitrogen flow. In the second step, the silicon nitride surface was activated with a piranha solution (1/3 hydrogen peroxide, H$_2$O$_2$, and 2/3 sulfuric acid, H$_2$SO$_4$) for 30 min. The piranha solution was in contact only with the Si$_3$N$_4$ surface in order to protect the backside of the working electrode preventing the aluminum etching. The piranha activation generates silanol (Si–OH) and silylamine (Si–NH) groups [23] onto the silicon nitride surface, which led to a good adhesion of the derivative membrane of copper phthalocyanine Cu(II) Pc-PAA. Finally the working electrode was abundantly washed with distillated water and dried under nitrogen flow. The Cu(II)Pc-PAA solution in DMSO (5 mg/mL) was diluted with THF to obtain 1 mg/mL of ionophore solution. Then, 30µL of the dilute solution was dropcasted onto the activated surface of Si$_3$N$_4$ and then dried at room temperature for 24 hr.

3. Surface and Morphological Characterization

3.1. Contact Angle Measurements

To control each modification step, the working electrode surface was characterized before and after each functionalization procedure by Contact Angle Measurements (CAM). The contact angles were determined from the droplet image using the tangent method. The liquid was deposited on solid surfaces with a micrometric syringe and controlled by means of a camera. Figure 3 presents the results of the water CAM of a bare Si$_3$N$_4$ surface, after piranha treatment and after functionalization with Cu(II) Pc-PAA.

The hydrophilicity of the surface substrate increased significantly after the piranha treatment as the CAM has decreased from 638 for a bare Si_3N_4 to 248 after piranha treatment (Figure 3B). This was due to the formation of the hydroxyl groups onto the silicon nitride surface. These would help to attach the polymeric membrane afterwards. The phtalocyanineCu(II)Pc-PAA was then dropcasted onto the activated silicon nitride surface. This was confirmed by the increase of CAM to 32° after functionalization (Figure 3C). The hydrophilic character was retained, even with a small increase in the CAM. This confirms a successful deposition of the polymeric membrane onto silicon nitride surface. The hydrophilicity was due to the presence of hydroxyl groups in the phtalocyanine membrane, whereas the small increase in the CAM was attributed to the presence of aromatic rings that contained carbon atoms.
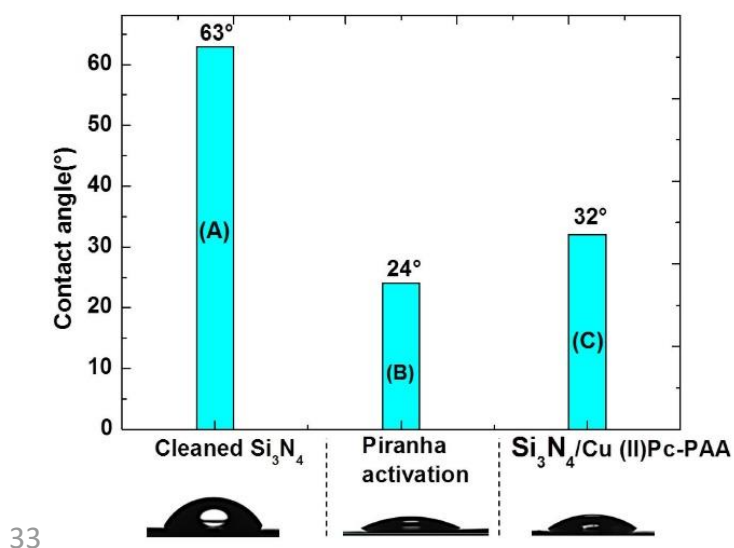

Fig. 3. Water contact angle measurements of bare Si_3N_4 surface (A), after piranha treatment (B), and after surface modification with membrane copper phthalocyanine (C). Below: images of 5 µL water droplet evolution onto silicon nitride surface at each step of its chemical surface modification.

3.2. Atomic Force Microscopy Characterization

The AFM images for the bare electrode and for the Cu (II)Pc-PAA deposited membrane in the surface of the silicon nitride Si_3N_4 are shown in Figure 4 A and Figure B, respectively. The bare silicon nitride showed a homogenous surface with a RMS roughness of 0.088 nm. This confirms the smooth aspect of silicon nitride surface. After being functionalized with phtalocyanine, the topography of the surface has totally changed and presents a homogenous morphological character of the polymeric membrane with a roughness of 7.53 nm. The texture and the ripple of the polymeric surface were very pronounced and they gave a tridimensional aspect to the surface of Cu(II)Pc-PAA. This was very important for the sensitivity of the membrane as the higher the surface roughness, the greater the number of surface sites were available and thus the chemical sensor would become more sensitive.
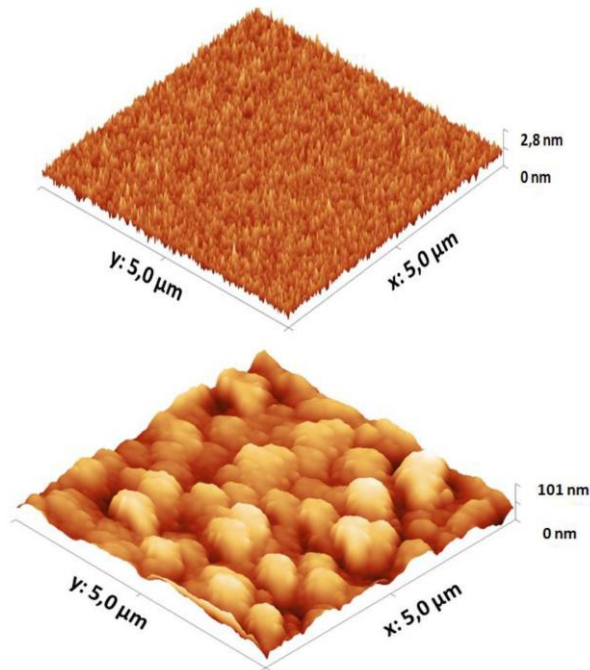
Fig. 4. AFM image, bare transducer Si_3N_4 (A) and transducer $Si_3 N_4$ after modification surface with membrane copper phthalocyanine (B).

4. Results and Discussion

4.1. Effect of Frequency

Typical C(V) curves with different frequencies ranging from 100 Hz to 10 kHz of the capacitive chemical sensor recorded in a Tris-HCl buffer solution 0.1 M at pH 7.2 are presented in Figure 5. At the quasi-static frequencies of 100 Hz, the capacitance curves of this structure showed a well-known low-frequency behavior with typical accumulation, depletion and inversion regions [24]. The capacitance rose up to C_{max} by decreasing the frequency in the inversion region. At a quasi-static frequency, the C_{max} in the inversion region was similar to C_{max} in the accumulation region. Similar effects were observed in the capacitance structures modified with selective membranes [25, 26].
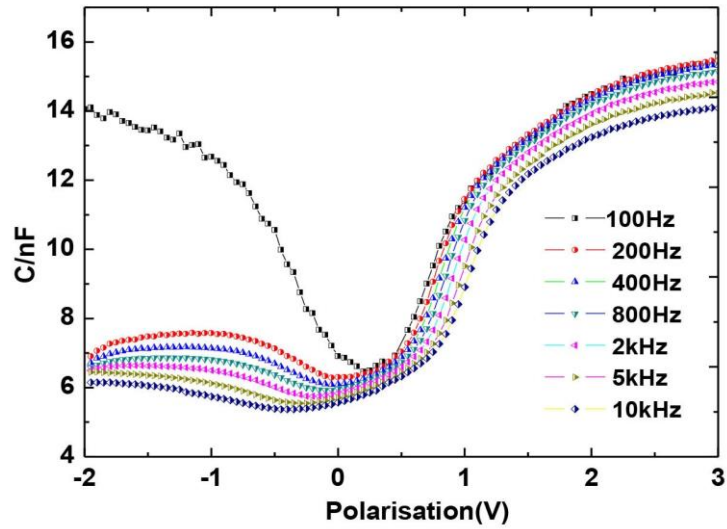
Fig. 5. Capacitance measurements (C) as a function of potential (V) for different frequency ranges for EIS structure.

Similarly, the capacitance measurements for the chemical sensor were performed in Tris-HCl buffer solution 0.1 M at pH 7.2 at high and quasi-static frequency from -2 V to 3 V. Figure 6, illustrates the vastly different characteristics of the CV curves measured at high and quasi-static frequency for a p-type semiconductor. The capacitance depends on the voltage value applied to the device structure [27]. The three regions associated with this graph were accumulation, depletion, and inversion [28]. Therefore, at high frequency, the generation time of the pair electron-hole and the creation of an inversion layer could not follow the applied potential to the device.
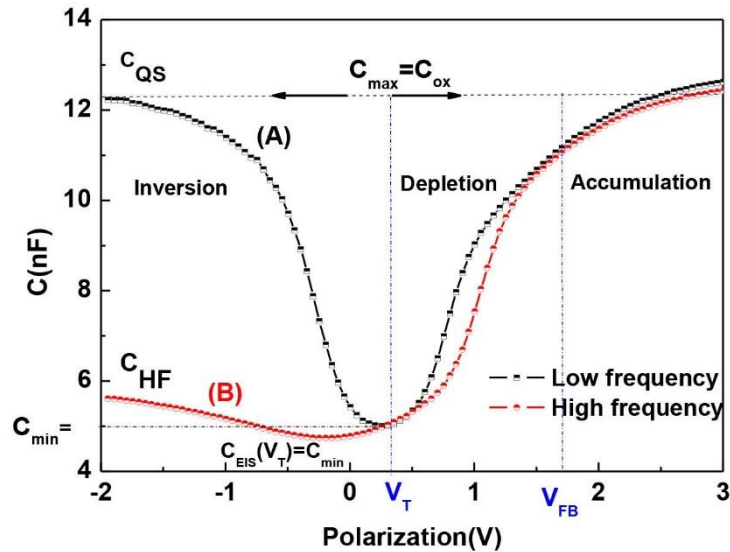

Fig. 6. C-V curves obtained by using Mott-Schottky analysis. The potential applied to the capacitance chemical sensor at (A) quasi-static measuring frequency and at (B) high frequency, C_{max}: maximum capacitance of structure, C_{QS}: quasi-static capacitance, C_{HF}: high-frequency capacitance, C_{min}: minimum capacitance of structure, V_{FB}: flat band voltage, V_T: threshold voltage.

Thus, once the depletion reached its maximum width, the capacitance structure (C) measured at high frequency would be based only on the distribution of the majority carriers (hole). Under these conditions, the total capacity measured at high frequencies was the capacitance of the silicon oxide layer (C_{ox}) in series with another capacitance associated to the maximum depletion zone [29]. Finally, the total capacity of the structure would reach a minimum and it would be independent from the applied voltage.

At low frequencies, in the inversion zone, when the electrons could follow the applied potential, the maximum capacitance would correspond to the capacity of the oxide and it would be a similar capacitance in the case of accumulation zone. Hence, the characteristic C(V) in the inversion region would depend on the frequency according to the minority carriers able to follow the applied potential.

In this case, two capacitances should be considered, one relating to the space charge regions and the other for the double layer. Since the capacitances were in series, the total capacitance was the sum of their reciprocals. As the space charge capacitance was much smaller than the double layer capacitance, the double layer capacitance contribution to the total capacitance was negligible. Consequently, the capacitance value calculated from this model was assumed to be the value of the space charge capacitance.

4.2. <u>pH Sensitivity of the Al-Cu/Si–p/SiO$_2$/Si$_3$N$_4$ Transducer</u>

In this study, the silicon nitride (Si$_3$N$_4$) substrate was used due to its high stability, low drift, low permeability and low structural porosity. Therefore, the capacitance structure AlCu/Si-p/SiO$_2$/Si$_3$N$_4$ was tested first for pH measurements [30, 31] in order to validate its behavior toward H$^+$ ions. Then, the same transducer was used for phosphate detection using a sensitive membranes [32].

Silicon nitride surface was characterized only in Tris solution within the pH range pH 4 to pH 10. Figure 7 A represents a set of Mott-Schottky curves of bare silicon nitride at different pH. Here, the horizontal shift of the flat band voltage (ΔV_{FB}) was increased toward positive values by decreasing the pH. This change of the flat band voltage (ΔV_{FB}) could be explained by the presence of both H$^+$ and Si-NH$_2$ groups at the sensors surface [24]. The pH sensitivity was calculated from the slope of the flat band voltage [33], which was obtained from Mott-Schotky curves (Figure 7B). Here, the average Nernstian sensitivity was 51 mV/pH, which was in good agreement with the results obtained in the literature using Si$_3$N$_4$ pH sensors (Table 1). This pH test allowed checking the good capacitance structure and the working electrode interactivity.

Table 1. Performances of some Si$_3$N$_4$ pH sensors reported in the literature.

Tranducer	Sensitivity	Reference
SiO$_2$/Si$_3$N$_4$ ISFET	54 mV/pH	[23]
Si$_3$N$_4$ ISFET	46 mV/pH	[34]
Si$_3$N$_4$ ISFET	50.1mV/pH	[35]
Al/p-Si /SiO$_2$/Si$_3$N$_4$	51mV/pH	This work

4.3. pH Effect on the Phosphate Detection

The phosphate phtalocyanine sensitive membrane was drop casted onto the activated silicon nitride surface, as previously described. Accordingly, the phosphate ions HPO_4^{2-} were detected at 10^{-8} M within the range of pH 5 to pH 10. The pH adjustments were tested in Tris-HCl buffer (0.1 M). The same behavior of pH variation was observed for the Mott-Schottky analyses (Figure 8 A). The variation of the flat band voltage (ΔV_{FB}) was plotted versus pH and showed almost stable potential between pH 7 and pH 8 (Figure 8B). The variation of the potential at pH $\leq$ 7 could be related to the protonation of the ionophore in the membrane which resulted in a loss of its ability to interact with HPO_4^{2-} ions [36,37]. At higher pH (>8.0), the potential increasing may be attributed to the formation of hydroxyl-complexes of Cu^{2+} in solution. For the rest of the analyses, the phosphate detection was made in pH 7.2 as it was in the range of pH where the potential was found stable. Moreover, this pH was close to the pH of the physiological mediums which give the possibility to perform ions detection complex environments.
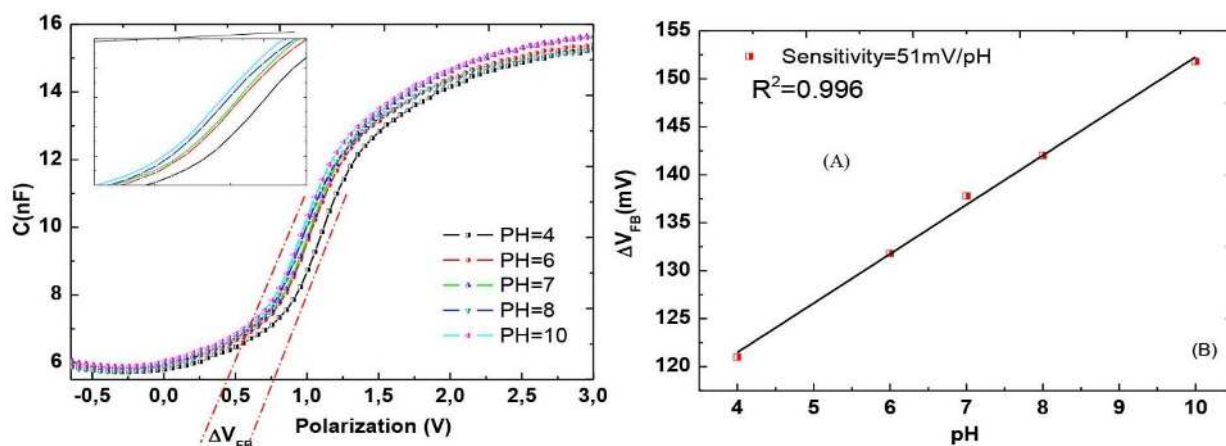

Fig. 7. (A), pH response of AlCu/Si-p/SiO₂/Si₃N₄ chemical sensor (B), Sensitivity of chemical sensor versus different pH values.
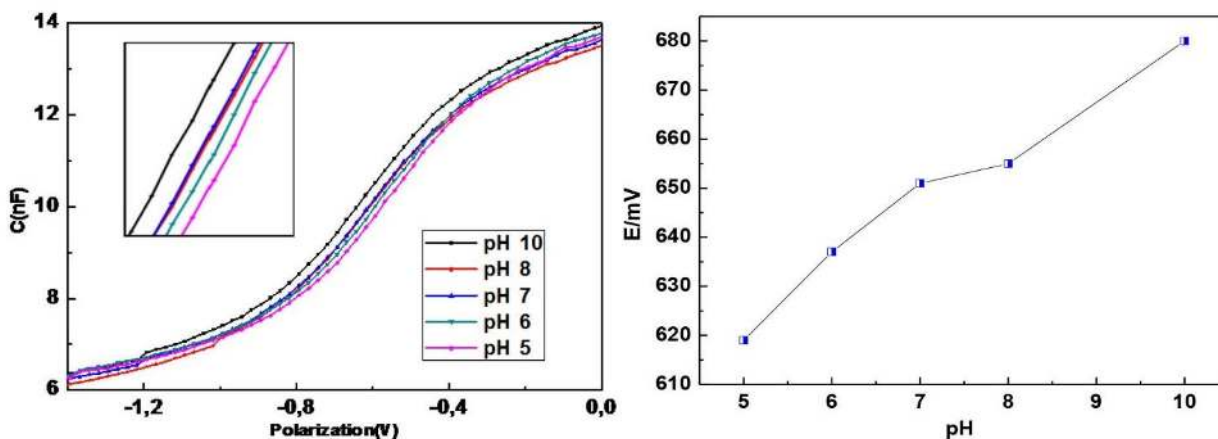

Fig. 8. pH effect on the flat band potential response of the Cu(II)Pc-PAA modified AlCu/Si-p/SiO₂/Si₃N₄ chemical sensor for phosphate detection.

4.4. Mott-Schottky Analysis for Bare and Functionalized Chemical Sensors

The adsorption of the Cu(II)Pc-PAA layer was characterized by the capacitance voltage method at a fixed frequency of 10 kHz. The measurements were performed in Tris-HCl buffer solution (pH 7.2) in a Faraday cage at room temperature.

Figure 9 shows the CV measurements of the sensor before and after functionalization with Cu(II)Pc-PAA membrane. Indeed, the total capacitance C in the accumulation region has dramatically decreased after the deposition of the sensitive membrane Cu(II)Pc-PAA onto the transducer. This was due to an increase in the insulator thickness after dropping this material. The capacity was inversely proportional to the thickness according to the following equation [14]:

where C is the capacitance of the structure, $\varepsilon = \varepsilon_0 \varepsilon_r$ or ε_0 is the dielectric permittivity of the vacuum, ε_r is the dielectric permittivity of the insulator, S is the surface of the working electrode, and ε is the insulator thickness.
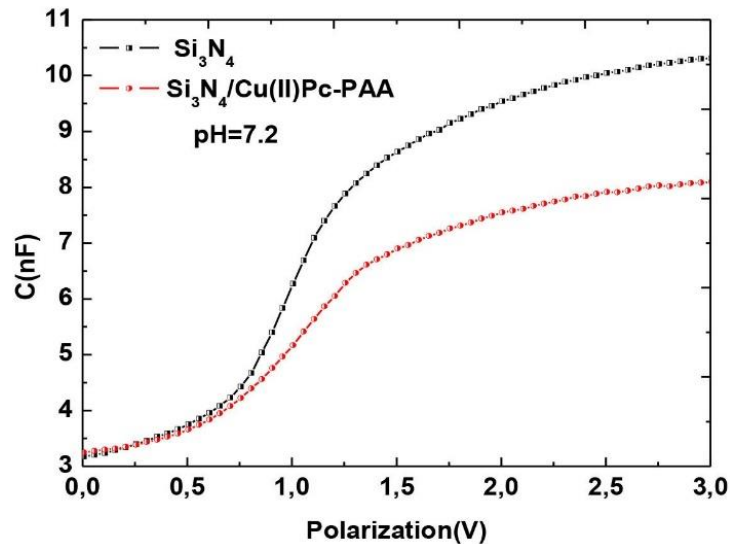

Fig. 9. Mott-Schottky analyses for bare AlCu/Si-p/SiO$_2$/Si$_3$N$_4$ and Cu(II) Pc-PAA modified capacitance chemical sensor in Tris buffer solution of pH 7.2.

4.5. Functionalized EIS Structure Response Towards HPO$_4^{2-}$ Ions

After optimizing all different parameters in different conditions, the capacitive chemical sensor was tested for the detection of phosphate ions by capacitance measurements. Therefore, the AlCu/Si-p/SiO$_2$/Si$_3$N$_4$/Cu(II)Pc-PAA structure was tested for different HPO$_4^{2-}$ concentrations and at a fixed frequency of 10 kHz, as presented in Fig.10. Subsequently, a significant variation of the potential of the flat band voltage V$_{FB}$ in the depletion range was observed by increasing HPO$_4^{2-}$ concentration. This could be explained by the change of the potential at the surface after the axial ligation of HPO$_4^{2-}$ to the metallic center (which is copper (Cu) in this study) of the phthalocyanine derivative [38]. In

addition, a slight change of capacitance in the regime of accumulation was noticed and was accompanied with a V_{FB} variation. This change was clearly related to the dielectric constant and the thickness changes due to the adsorption of charged species at the Cu (II)-Pc-PAA membrane surface.

To determine the HPO^2_4 sensor sensitivity, the V_{FB} variation (ΔV_{FB}) was plotted as a function of HPO_4^{2-} concentration (Fig. 10B). A comparison with data available from literature for other types of phosphate sensors is presented in Table 2. Here, the Al/Si p/SiO$_2$/Si$_3$ N$_4$/Cu(II)Pc-PAA based chemical sensor presented in this work has shown a sensitivity of 27.7 mV/decade at high frequency 10 kHz and 32mV/decade at quasi-static frequency 100 Hz for phosphate ions detection. This chemical sensor was tested in a large phosphate concentration range and proving a low detection limit of 1 nM.

The sensitivity from the slope of the linear part was calculated at 27.7 mV/decade, which was in good agreement with the Nernstian behavior for divalent ions. The obtained results allowed to confirm the interesting performances for the HPO_4^{2-} detection using the new receptor material (Cu(II)-Pc-PAA). Compared to other developed phosphate sensor [10], the detection limit was 1 nM within the detection range of 10^{-10} M to 10^{-6} M.

The increase of the capacitance depends on the ability of the electron concentration to follow the applied AC signal. This happens only at low frequencies where the recombination-generation rates of minority carriers (in our example, electrons) can keep up with the small-signal variation and lead to charge exchange with the inversion layer during the signal measurements. Unlike depletion and weak inversion, at strong inversion the incremental charge is no longer at the edge of the depletion region but at the semiconductor surface inversion layer, resulting in a large capacitance [26]. Experimentally, the range in which the capacitance is most frequency dependent was found between 100 Hz and 10 kHz for the capacitance structures. This is related to the carrier lifetime in the silicon substrate. As a consequence, capacitive curves measured at higher frequencies do not show the increase of capacitance in strong inversion [27].

Table 2. Performances of some phosphate ion sensors reported in the literature.

Interface	Electrochemical technique	Detection limit (mM)	Linear range (mM)	References
PyO/nano-CPGCE	Stirred batch amperometry	0.3	1 to 100	[39]
Co m-electrode	Potentiometry	< 10	10 to10000	[40]
PB-GCE	Differential pulse voltammetry	38.3	500 to 5000	[41]
GLA-PyO-CoPC-SPE	Stirred batch amperometry	2.28	2.5 to 50	[42]
Gold rotating electrode	Stirred batch amperometry	0.11	0.59 to 3.49	[43]
CB-SPE	Stirred batch amperometry	0.1	0.5 to 100	[44]
CB-SPE	Continuous flow amperometry	6	10 to 80	[45]
Al-Cu/Si-p/SiO$_2$/Si$_3$N$_4$/ Cu(II)Pc-PAA at 10 kHz frequency	Capacitance-voltage	0.001	0.0001 to 1	This work
Al-Cu/Si-p/SiO$_2$/Si$_3$N$_4$/ Cu(II)Pc-PAA at 100 Hz frequency	Capacitance-voltage	0.001	0.0001 to 10	This work

PyO : Pyruvate Oxidase; SPE: Screen Printed Electrode; CoPc/SPCE: Cobalt (II) phthalocyanine/Screen printed carbon electrode.
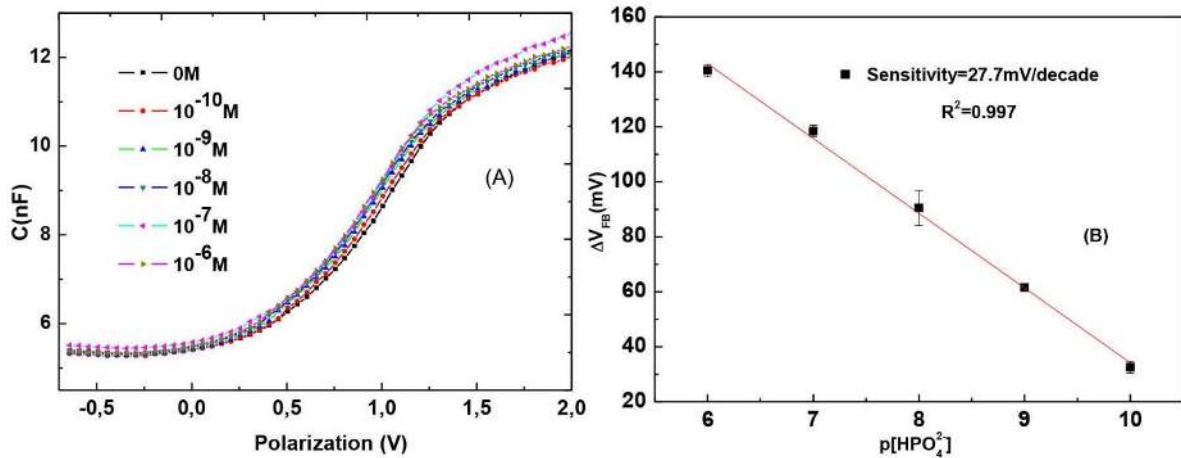
Fig. 10. (A) Variation of capacitance various potential for AlCu/Si-p/SiO$_2$/Si$_3$N$_4$ structure functionalized with a Cu (II) Pc-PAA for 19 different phosphate ion concentrations. Buffer solution, Tris-HCl 10 mM, pH 7.2, f= 10 kHz. (B) Sensor sensitivity.
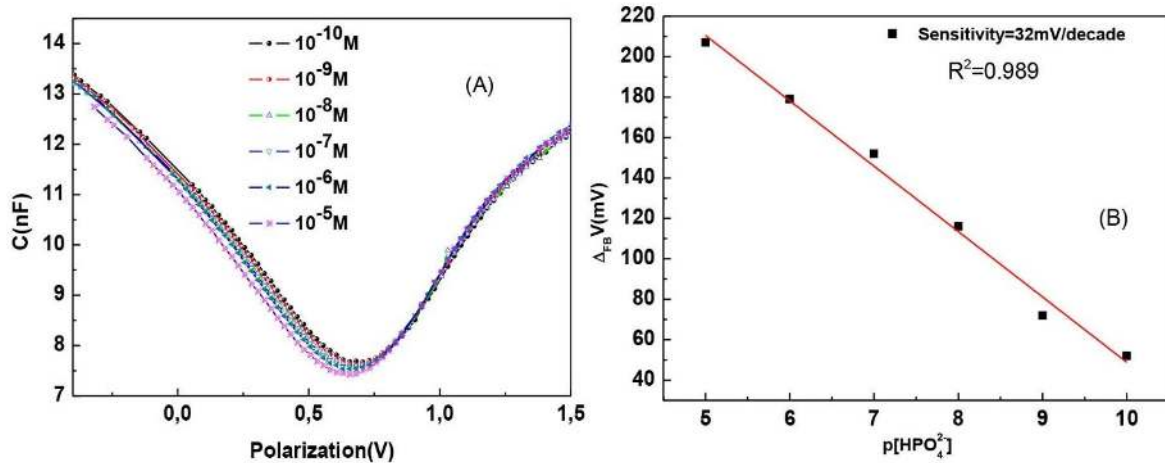

Fig. 11. (A) The variation of flat band potential of AlCu/Si-p/SiO$_2$/Si$_3$N$_4$/Cu(II)Pc-PAA structure plotted versus phosphate ion concentrations, buffer solution, Tris-HCl 10 mM, pH 7.2, f= 100 Hz (B) Sensitivity of the sensor as function of phosphate ion concentrations.

The same study of phosphate detection was performed within the same range potential at low frequency of 100 Hz (Figure 11). In the inversion regime, the capacitance at extremely low frequencies of the order of some Hz, suffers from too much noise or parasitic capacitances. If there are many electrons at the oxide semi-conductor interface (in inversion regime for capacitance structure with a p-type substrate), there would be transition probability of the semiconductor electrons to the traps in the oxide. This probability would depend on the distance between the loads and the semiconductor-insulator interface area, as well as the barrier height between the two states.

Figure 11A shows the C(V) curves with ΔV_{FB} as a parametric variable. This shifted along the voltage axis without any change in their shape. The flat-band voltage shift was plotted as a function of the concentration of phosphate ions. Figure 11B, illustrates the chemical sensor response near the Nernstian response, equal to 32 mV/ decade.

4.6. Interference Study

The specificity is one of the most important characteristics of a chemical sensor. The capacitance chemical sensor AlCu/Si-p/SiO$_2$/Si$_3$N$_4$/Cu(II)Pc-PAA has demonstrated a higher preference for HPO$_4^{2-}$ ions when compared to other examined ions such as chloride Cl$^-$, sulfate SO$_4^{2-}$, carbonate CO$_3^{2-}$ and perchlorate ClO$_4^{2-}$ [36]. The flatband voltage shift ΔV_{FB} of these interferences was plotted and compared to the responses of HPO$_4^{2-}$ (Figure 12). The linear parts of the potential responses of the chemical sensors for all other ions were much lower when compared to the main ion HPO$_4^{2-}$.
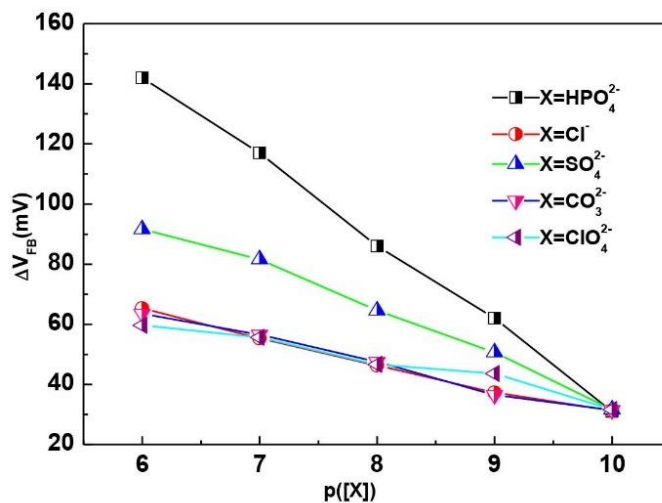

Fig. 12. Evolution of depletion capacitance as a function of Cl$^-$, SO$_4^{2-}$, CO$_3^{2-}$ and ClO$_4^{2-}$ ions. Test solution Tris 10 mM and pH 7.2.

The sensitivity of ions adsorbed onto receptor layer copperphthalocyanine Cu(II)Pc-PAA is presented in Table 3. Here the new material Cu(II)Pc-PAA was highly sensitive for phosphate ions when compared to the other interferences. As all other interfering ions were also detected at 10^{-10} M, the chemical sensor could be classified as selective for phosphate ions from 10^{-9} M.

Table 3. Specificity of phosphate adsorption onto copper phthalocyanine Cu(II)Pc-PAA capacitance chemical sensor.

Target ion	Sensitivity (mV/decade)
Cl$^-$	8.6
SO$_4^{2-}$	15
CO$_3^{2-}$	8.4
ClO$_4^{2-}$	6.8
HPO$_4^{2-}$ at F=10 kHz	27.7
z	32

5. Conclusion

The capacitive electrochemical ion sensor has been developed in the present study using a new derivative copper phthalocyanine Cu(II)-Pc-PAA as sensitive layer for phosphate ion detection. The capacitance structure of the chemical sensor has been based on $AlCu/Si-p/SiO_2/Si_3N_4$, which is a stable configuration and stable combination of materials for electrochemical measurements. The behavior of the capacitance structure has been studied at low and high frequencies for the detection of phosphate ions. These ions have been detected by the variation of the capacitance as function of the applied potential (C (V)) using the Mott-Schottky technique. The phosphate ions were detected selectively within the range (10^{-10} to 10^{-5} M) and the limit of detection has been found to be 1 nM. These improved performances have been explained by the physical properties of the capacitance structure of the WE, the Nernstian sensitivity, and repeatability of measurements. The specificity of the $AlCu/Si-p/SiO_2/Si_3 N_4/Cu(II)Pc-PAA$ chemical sensor has been also investigated in relation to other interfering ions: Cl^-, SO_4^{2-}, CO_3^{2-} and ClO_4^{2-}. This could be very promising and was suitable for the study of the removal of phosphate in rivers, lakes, and seas.

References

[1] B. Geissler, M. C. Mew, O. Weber, G. Steiner, *Resour Conserv Recy Part B* **2015**, 105, 246–258.
[2] R. al Rawashdeh, P. Maxwell, *Mineral Econ* **2011**, 24, 15, 27.
[3] N. Mokadem, Y. Hamed, A. B. Sâad, I. Gargouri, *AJG* **2014**, 7, 2071–2079.
[4] F. Ogata, A. Ueda, S. Tanei, D. Imai, N. Kawasaki, *Ind. Eng. Chem* **2016**, 35, 287–294.
[5] F. Kivlehan, W. J. Mace, H. A. Moynihan, D. W. M. Arrigan, *Anal. Chim. Acta* **2007**, 585, 154–160.
[6] J. Nie, J.-P. Li, H. Deng, H.-C. Pan, Chin. *J. Anal. Chem* **2015**, 43, 609–617.
[7] J. Payandeh, D. L. Minor Jr, *J. Mol. Biol* **2015**, 427, 3–30.
[8] W. Bala, M. Wojdyla, M. Rebarz, M. Szybowicz, M. Drozdowski, A. Grodzicki, P. Piszczek, *JOAM* **2009**, 11, 264– 269.
[9] S. Shahrokhian, M. Ghalkhani, M. K. Amini, *Sens. Actuators, B* **2009**, 137, 669–675.
[10] S. Shahrokhian, *Anal. Chem* **2001**, 73, 5972–5978.
[11] J. Rossignol, G. Barochi, B. de Fonseca, J. Brunet, M. Bouvet, A. Pauly, L. Markey, *Sens. Actuators, B* **2013**, 189, 213–216.
[12] Y.-Q. Zhang, Y.-J. Fan, L. Cheng, L.-L. Fan, Z.-Y. Wang, J.-P. Zhong, L.-N. Wu, X.-C. Shen, Z.-J. Shi, *Electrochim. Acta* **2013**, 104, 178–184.

[13] K. I. Ozoemena, T. Nyokong, *Electrochim. Acta* **2006**, 51, 5131–5136.

[14] M. Braik, C. Dridi, A. Ali, M. N. Abbas, M. Ben Ali, A. Errachid, *Org Electron* **2015**, 16, 77–86.

[15] K. I. Ozoemena, T. Nyokong, *Talanta* **2005**, 67, 162–168.

[16] L. Chen, T. Wang, Y. Zhao, X.-R. Zhang, *Energy Convers. Manage* **2014**, 79, 317–333.

[17] H. Dang, X. Wu, X. Sun, R. Zou, R. Zhang, S. Yin, *JoS* **2015**, 36, 104003.

[18] F. I. Bohrer, C. N. Colesniuc, J. Park, M. E. Ruidiaz, I. K. Schuller, A. C. Kummel, W. C. Trogler, *J. Amer. Chem. Soc* **2009**, 131, 478–485.

[19] J.-Z. Li, X.-C. Wu, R. Yuan, H.-G. Lin, R.-Q. Yu, *Analyst* **1994**, 119, 1363, 1366.

[20] M. N. Abbas, A. L. A. Radwan, N. M. Nooredeen, M. A. A. El-Ghaffar, *J. Solid State Electrochem* **2016**, 20, 1599–1612.

[21] H. A. Moynihan, G. Claudon, *Cryst.Eng.Comm* **2010**, 12, 2695–2696.

[22] M. A. A. El-Ghaffar, N. R. El-Halawany, H. A. Essawy, *J. Appl. Polym. Sci* **2008**, 108, 3225–3232.

[23] B. Hajji, P. Temple-Boyer, J. Launay, T. do Conto, *Microelectron Reliab* **2000**, 40, 783–786.

[24] M. Bougrini, A. Baraket, T. Jamshaid, A. E. Aissari, J. Bausells, M. Zabala, N. E. Bari, B. Bouchikhi, N. Jaffrezic-Renault, E. Abdelhamid, N. Zine, *Sens. Actuators, B* **2016**, 234, 446–452.

[25] M. H. Abouzar, W. Moritz, M. J. Schöning, *Phys. Status Solidi A* **2011**, 208, 1327–1332.

[26] B. Rong, L. K. Nanver, J. N. Burghartz, A. B. M. Jansman, A. G. R. Evans, B. S. Rejaei, *ESSDERC* **2003**, 489–492.

[27] W. M. Siu, R. S. C. Cobbold, *IEEE Trans. Electron Devices* **1979**, 26, 1805–1815.

[28] P. Fabry, L. Laurent-Yvonnou, *Anal. Chim* **1990**, 286, 23–40.

[29] A. Demoz, E. M. J. Verpoorte, D. J. Harrison, *J. Electroanal. Chem* **1995**, 389, 71–78.

[30] P. Bergveld, *IEEE Trans Biomed Eng* **1972**, 19, 342–351.

[31] F. V. Gasparyan, A. Poghossian, S. A. Vitusevich, M. V. Petrychuk, V. A. Sydoruk, J. R. Siqueira, O. N. Oliveira, A. Offenhausser, M. J. Schoning, *IEEE Sensors J* **2011**, 11, 142-149.

[32] S. Azzouzi, M. Ben Ali, M. N. Abbas, J.Bausells, N. Zine, A. Errachid, *Org Electron* **2016**, 34, 200–207.

[33] L. Bousse, N. F. D. Rooij, P. Bergveld, *IEEE Trans. Electron Devices* **1983**, 30, 1263, 1270.

[34] B. D. Liu, Y. K. Su, S. C. Chen, *IJE* **1989**, 67, 59–63.

[35] S. Martinoia, G. Massobrio, L. Lorenzelli, *Sens. Actuators, B* **2005**, 105, 14–27.

[36] M. R. Ganjali, P. Norouzi, N. Hatambeygi, M. SalavatiNiasari, *J. Braz. Chem. Soc* **2006**, 17, 859–865.

[37] P. Kumar, D. M. Kim, M. H. Hyun, Y.-B. Shim, *Talanta* **2010**, 82, 1107–1112.

[38] C. M. Drain, J. T. Hupp, K. S. Suslick, M. R. Wasielewski, X. Chen, *J. Porphyr. Phthalocyanines JPP* **2002**, 06, 243–258.

[39] M. A. Rahman, D.-S. Park, S.-C. Chang, C. J. McNeil, Y.-B. Shim, *Biosens. Bioelectron* **2006**, 21, 1116–1124.

[40] Z. Zou, J. Han, A. Jang, P. L. Bishop, C. H. Ahn, *Biosens. Bioelectron* **2007**, 22, 1902–1907.

[41] L. Torrezani, A. A. Saczk, M. Firmino de Oliveira, N. R. Stradiotto, L. L. Okumura, *Electroanalysis* **2011**, 23, 2456– 2461.

[42] L. Gilbert, A. T. A. Jenkins, S. Browning, J. P. Hart, *Sens. Actuators, B* **2011**, 160, 1322–1327.

[43] J. Jonca, W. Giraud, C. Barus, M. Comtat, N. Striebig, D. Thouron, V. Garçon, *Electrochim. Acta* **2013**, 88, 165–169.

[44] D. Talarico, F. Arduini, A. Amine, D. Moscone, G. Palleschi, *Talanta* **2015**, 141, 267–272.

[45] D. Talarico, S. Cinti, F. Arduini, A. Amine, D. Moscone, G. Palleschi, *Environ. Sci. Technol* **2015**, 49, 7934–7939.